

CRUSTAL STRUCTURE OF THE EASTERN SNAKE RIVER PLAIN  
DETERMINED FROM RAY TRACE MODELING  
OF SEISMIC REFRACTION DATA

M. A. Sparlin<sup>1</sup> and L. W. Braile

Department of Geosciences, Purdue University, West Lafayette, Indiana 47907

R. B. Smith

Department of Geology and Geophysics, University of Utah  
Salt Lake City, Utah 84112

**Abstract.** Ray trace travel time modeling of the seismic refraction record sections for a profile from near Soda Springs, Idaho, to near McKay, Idaho, was used to derive a crustal model across the eastern Snake River Plain (ESRP). The derived crustal model is consistent with the velocity structure interpreted from a profile along the axis of the ESRP. The interpretation also indicates that significant lateral inhomogeneities exist in the upper crust beneath the ESRP when compared with the upper crust beneath the adjoining Northern Rocky Mountain and Basin and Range provinces. The most prominent features of the crustal structure inferred by the ray trace modeling are as follows: (1) The northwest margin of the ESRP was modeled as a fault structure, downthrown on the SRP side (SE) with an offset of greater than 4 km. The southeast margin, conversely, appears to be downwarped with possible minor faulting. Paleozoic sedimentary rocks are present beneath the Cenozoic volcanics of the ESRP possibly to and beyond 40 km from the southeastern margin of the ESRP near Blackfoot, Idaho. (2) The modeling indicates no abrupt variation in the depth to the top of the lower crustal layer near the margins of the ESRP. (3) An intermediate 6.5 km/s layer occurring beneath the ESRP, interpreted from a refraction profile located along the axis of the ESRP, was found to be localized within the ESRP margins. This layer is interpreted as a pervasive intrusion of higher velocity material from the upper mantle into the highly fractured upper crustal layer in this region. (4) A density model of the crust across the ESRP was prepared with the densities selected using the interpreted seismic velocities as a constraint. The gravity field calculated from this model resulted in a good match to observed gravity data over the eastern Snake River Plain.

#### Introduction

During the 1978 Yellowstone-Snake River Plain (Y-SRP) seismic profiling experiment, a partially reversed seismic refraction profile was recorded along a northwest-southeast line across the axis of the eastern Snake River Plain (ESRP). Four shotpoints located along this profile resulted

<sup>1</sup>Now at Arco Oil and Gas Company, Dallas, Texas 75221.

in refracted and reflected arrival phases, which have been interpreted in order to infer the crustal structure beneath the ESRP and the transition in crustal models between the ESRP and adjacent provinces. The objective of this paper is to describe ray trace travel time modeling applied to the seismic data recorded along this northwest-southeast line. In addition, the anomalous gravity field of the derived crustal model is compared with observed gravity data across the ESRP in order to confirm and further constrain the crustal model. The details of the 1978 Y-SRP seismic profiling experiment and shotpoint and seismograph information are presented by Smith et al. [this issue] and Braile et al. [this issue].

#### Data Acquisition and Presentation

Seismograph stations and shot locations for the eastern SRP phase of the Y-SRP seismic experiment are shown in Figure 1. Four shotpoints were recorded along the axis of the ESRP; SP5, SP8, SP4 and SP2; and four shotpoints along a profile approximately perpendicular to the ESRP axis; SP7, SP8, Gay Mine, and Conda Mine. Shotpoint 8 was recorded both transverse (NW-SE) and parallel (NE-SW) to the axis of the ESRP. Shotpoint locations, origin times, sizes, and other relevant information for these sources are given by Braile et al. [this issue]. The 196-km seismic refraction line oriented roughly perpendicular to the axis of the ESRP and intersecting both the northwest and southeast boundaries of the SRP near Arco and Blackfoot, Idaho, respectively, has been interpreted using ray trace modeling. This refraction profile will be termed the Conda-SP7 line or the 'crossline.' The interpretation procedure and the derived crustal model along this profile are the principal topics of this paper. In addition, a 47-km-long reversed profile from SP8 to SP4 near the center of the ESRP (Figure 1) was interpreted. This profile is particularly relevant to the Conda-SP7 interpretation because the two profiles intersect near the axis of the ESRP.

As described in detail by Smith et al. [this issue] and Braile et al. [this issue], seismic data were recorded along the Conda-SP7 profile utilizing portable seismographs with timing referenced to crystal clocks and radio signal WWV or the radio broadcast time standard WWVB. Seismograms recorded on FM tape or analog records (240 mm/min or 480 mm/min fast rotation smoked-paper drum recordings) were subsequently digitized for plotting as reduced-time record sec-

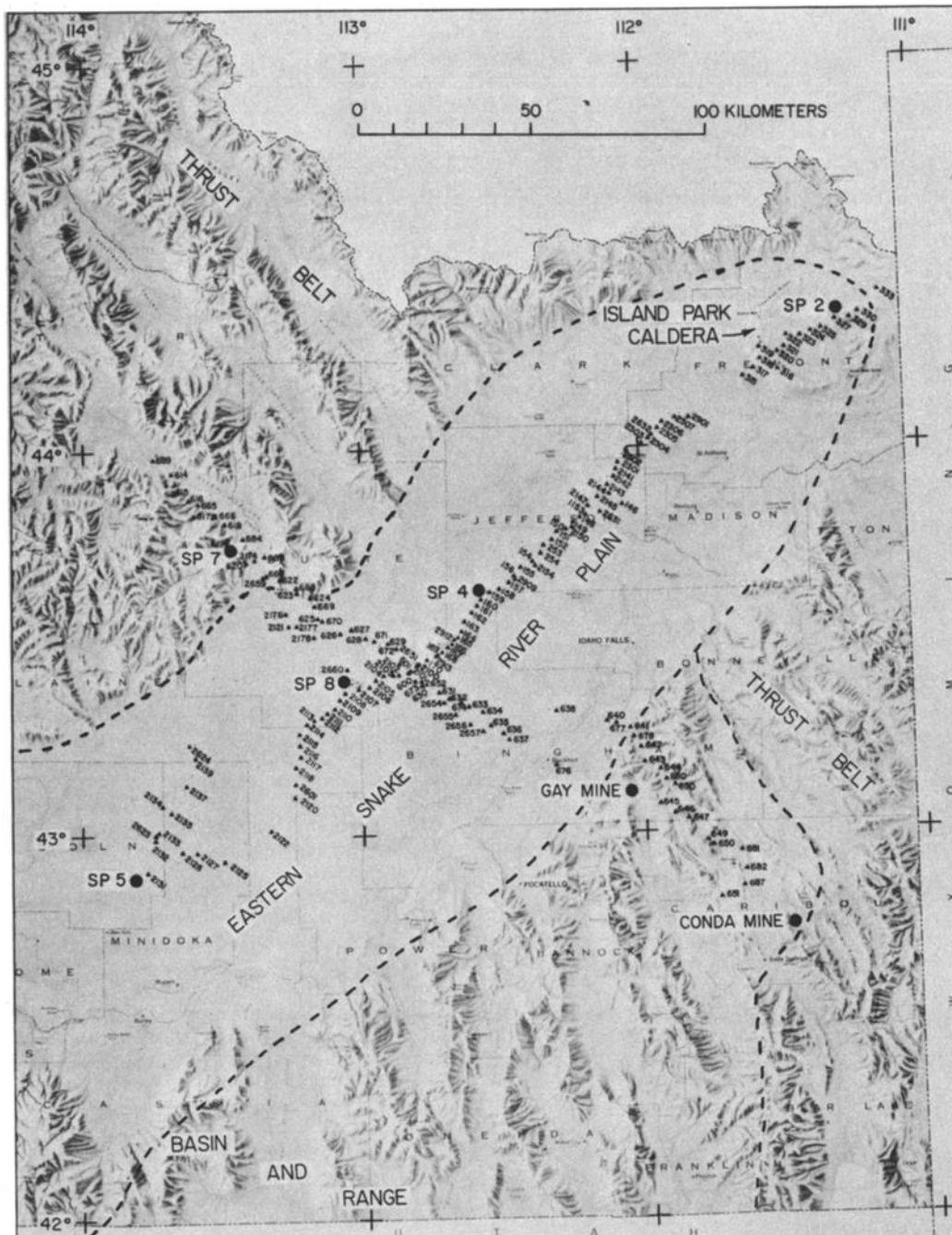


Fig. 1. Index map of southeastern Idaho showing locations of shotpoints (large circles) and seismograph stations (small triangles) utilized during the eastern Snake River Plain phase of the refraction experiment. Province boundaries (dashed lines) are from Fenneman and Johnson [1946].

tions. Data reduction and editing procedures were described by Schilly [1979].

In order to standardize the response of the seismograms on the plotted record sections to facilitate correlation of phases and reading travel times, all seismograms were normalized to a reference instrument, in this case a Sprengnether MEQ-800 seismograph with 0 to 5-Hz filter settings and an S-7000 seismometer set for a 1-Hz resonant frequency. Thus, the variations in response between the many recording systems utilized in the experiment were minimized which allowed for amplitude control

and improved the coherency of arrival character between seismograms. The amplitude normalization procedure was described by Baker et al. [this issue].

All of the seismograms presented here are vertical-component records which have been plotted with a reducing velocity of 6 km/s and time corrected to a 1200-m elevation datum utilizing an average velocity for the near-surface material of 4.50 km/s. Seismogram amplitudes were scaled for plotting by the source-receiver distance raised to the 1.5 power such that amplitudes of the arrivals at large distance are visible

on the record sections. In addition, a recursive bandpass filter was applied to each seismogram to pass frequencies from approximately 1 to 8 Hz [Baker, 1979].

#### Seismic Modeling Procedure

The procedure utilized in the interpretation of the Conda-SP7 refraction profile was to identify the travel times of principal refracted and reflected phases by their lateral coherency of amplitude and phase character of the seismograms. Because of the seismogram normalization procedure, phase correlation was usually significant except for (generally) small travel time shifts due to local velocity anomalies, elevation effects, or timing errors. A comment is appropriate here as to the identification of the arrival time of a phase on the observed record sections. We have consistently selected the onset of a phase, recognized by amplitude or frequency character, to be the earliest time consistent with the data. The largest amplitude of the arriving phase generally occurs 0.1-0.5 s after the onset time. Considering the band-limited source and recording instruments, this is the most appropriate convention for travel time modeling. Also, calculated arrival times were compared with expanded-amplitude (large scale) seismic record sections during the ray trace modeling. Examples of expanded-amplitude record sections are shown by Braile et al. [this issue]. These large-scale record sections were important in recognizing the true arrival times of several of the emergent phases which were observed. The seismic record sections shown here are designed to display the character of the seismograms for all phases, and thus the amplitudes are sometimes 'scaled down' such that onset times for first arrivals may not be apparent. Modeling of the correlated phases was initially performed using one-dimensional velocity models (travel times of reflected and refracted head wave arrivals for a stack of plane, homogeneous layers). This provided an approximate starting model beneath each shotpoint location from which to begin more complex travel time modeling. Subsequently, travel time calculations were performed by ray trace modeling [Cerveny et al., 1977] for each shotpoint and refraction profile.

In the ray-tracing modeling process, the velocity model was specified as homogeneous layers or bodies whose interfaces were described by spline fits to a series of grid points at which the velocity was specified. Seismic ray paths for both reflected and refracted primary arrivals were calculated by Snell's law ray tracing through the model. The results of the ray-tracing calculations were ray path diagrams and calculated travel times. The ray path diagrams were useful in the modeling process for correlation of travel time anomalies between the various record sections and for illustration of the wave propagation effects of the velocity model. Ray path diagrams are illustrated for the derived model in the figures which accompany each record section. The calculated travel times are geometrical ray theory times and are not necessarily represented by significant amplitude arrivals. The travel times are shown for

comparison on the observed record sections even if an arrival is not observed. After a satisfactory match between observed and theoretical arrival times was determined, by perturbation of the interfaces and velocities of the model for each record section, the portions of the model which were common to two or more record sections and two or more ray paths were adjusted until a satisfactory match to all of the data was obtained for a single model. Thus, the process required iterative refinement of the velocity model utilizing the seismic data from all of the crossline record sections and requiring consistency with the crustal model interpreted for the refraction profile along the axis of the ESRP (SP2-SP5 from Braile et al. [this issue]). Although this procedure is somewhat subjective and the models derived must be considered to be nonunique, the extensive modeling effort, as measured by the number of trial models utilized and the degree of structural perturbation of the various trial velocity models, produces confidence in the interpretation. In addition, many regions of the crustal model were traversed by ray paths from more than one shotpoint or for two or more ray types, and thus the derived model was subjected to a large number of travel time comparisons which were met in the successful velocity model.

The use of simple interfaces to represent the boundaries between the layers and bodies of the velocity model is a simplification for convenience of the travel time calculations and does not necessarily imply that the transition between the layers is a first-order discontinuity in velocity. In reality, these boundaries are probably thin velocity transition zones of about 0.1-1 km thickness. Such thin transition zones would be sufficient to nearly eliminate subcritical reflected arrivals on the record sections but would allow for prominent wide-angle reflected arrivals in accordance with the observed data. Thin velocity transition zones are present for the shallow volcanic layers, as indicated by the velocity well log for the ESRP (Figure 2). However, inclusion of these transition zones in the velocity model does not appreciably effect the travel time results.

In our modeling, we have also utilized nearly homogeneous layers and bodies for the velocity model. Of course, small velocity gradients are possible within these layers, but several observations indicated that any gradients would be small, and therefore we chose to model the crust with homogeneous layers. With the exception of arrivals from the volcanic layers, the record sections for the ESRP (the record sections shown here and by Braile et al. [this issue]) show small-amplitude first arrivals (refracted phases) followed by larger amplitudes interpreted to be wide-angle reflections. Presence of significant positive velocity gradients would produce large-amplitude first arrivals. Also, synthetic seismogram modeling by Braile et al. [this issue] of data recorded along the axis of the ESRP showed that homogeneous layer models were adequate to match the travel time and amplitude character of the observed data. The velocity structure of the shallow volcanic layers, however, is effectively a strong positive velocity gradient for the wavelengths of interest and is evident

by strong-amplitude arrivals from about 30–50 km distance on the ESRP record sections.

The advantage of the application of the ray trace theory in this case is the ability to simulate the propagation of various seismic wave types through discontinuous bodies and layers. In geometric ray theory a true head wave cannot be generated. For our travel time modeling, critical refractions were simulated by introducing a small (0.01 km/s/km) velocity gradient parallel to the interface along which the critical refractions were being calculated. Thus, with the extremely small curvature introduced into the ray as it traveled in the medium below the interface, quite accurate approximations to head wave arrivals could be obtained. The refractions simulated in this manner did not differ by more than 0.005 s in travel time when compared with travel times for plane homogeneous layered models computed using standard Snell's law methods.

In the diagrams to follow, the crustal velocity models are idealized, utilizing a simple linear or curvilinear boundaries and are thus approximations to a geological model. When more than one refracted phase appears on a plot, each phase was calculated separately with the velocity gradient introduced only in the layer in which the head wave was generated. The layers above and below were seismically homogeneous. The reflected phases were calculated with all layers homogeneous.

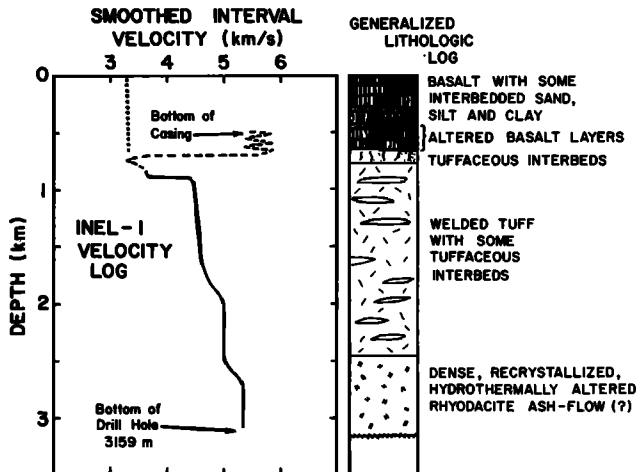


Fig. 2. Compressional velocity versus depth profile inferred for the shallow structure of the ESRP from the smoothed interval-velocity log observed in drill hole INEL-1. A generalized lithologic log from drill cuttings and cores [Doherty et al., 1979] is also shown. The interval-velocity data were available between the bottom of the drill casing and the bottom of the hole. However, the velocity data were highly erratic in the depth range of 500–800 m corresponding to a depth interval characterized by alternating layers of high-velocity altered basalts and low-velocity sedimentary rocks. The velocity data in this interval are shown schematically by the dashed line. The velocity profile for the upper 700 m which was used for interpretation (dotted line) is more consistent with the observed refraction data and the interpretations of Ackermann [1979] and Perkins et al. [1947].

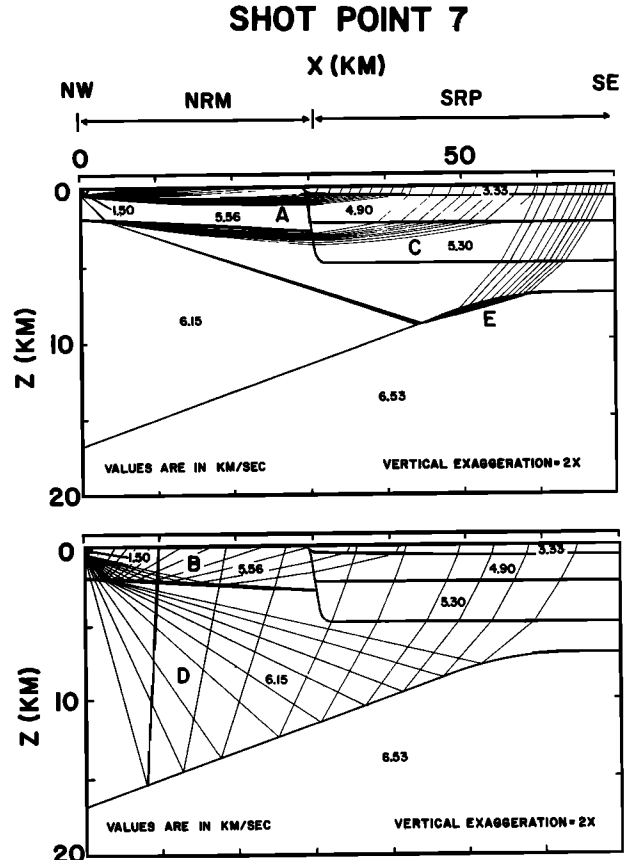


Fig. 3. Velocity model for the ESRP from shot-point 7 to the southeast showing the compressional wave velocities, interfaces (heavy solid lines), and computed ray paths (thin lines) for selected angle of incidence ranges for refracted (upper plot) and reflected (lower plot) ray types. The phase names correspond to calculated ray trace travel times shown in the record section in Figure 4.

In addition to the interpretation of the Conda-SP7 profile, the seismic refraction profile recorded along the axis of the ESRP (shot-points 5, 8, 4 and 2; Figure 1) was used to provide important constraints on the crustal model across the ESRP [Braile et al., this issue]. The 252-km reversed profile from shotpoint 2 to shotpoint 5 provided detailed information less complicated by lateral velocity structure variations. Because of the length of the SP2-SP5 profile and the shotpoint locations, this profile was particularly useful in determining the velocity-depth relations for the deeper layers beneath the ESRP.

Utilizing the interpretation of the SP2-SP5 profile [Braile et al., this issue], the following constraints were applied to the crustal model beneath the central area of the ESRP. The upper crustal layer (velocity  $\approx 6.15$  km/s) is interpreted to thicken toward shotpoint 2. The interpretation of the axial profile (shot-points 5, 8, 4 and 2; Braile et al. [this issue]) indicated an apparent velocity of the upper crustal layer of between 6.08 and 6.19 km/s. A value of 6.15 km/s was utilized in the ideal-

ized model of the Conda-SP7 profile presented here. Below the upper crustal layer and extending down to approximately  $19 \pm 1$  km is an intermediate layer with a velocity of approximately 6.53 km/s. The velocity of this layer is well defined from the interpretation of the shotpoint 2 to 5 data. The lower crust extends from the base of the intermediate layer to a depth of approximately  $42 \pm 2$  km with a velocity of 6.80 km/s.

For the near-surface volcanic structure, we relied heavily upon the interpretation of the INEL-1 well, 15 km from the northwestern boundary of the ESRP, east of Arco [Doherty et al., 1979]. This well penetrated to a depth of 3.16 km and intersected three general lithologies. Basalt interbedded with lacustrine and fluvial deposits was encountered from the surface to a depth of approximately 700 m. Below the surficial basalt, to a depth of 2400 m, a sequence of welded tuff was penetrated, and then from this level to the bottom of the well, recrystallized, hydrothermally altered rhyodacite was the predominant lithology [Doherty et al., 1979]. We utilized a velocity of 3.33 km/s in the idealized model for the surficial basalts and sedimentary deposits. This velocity is between the values of 3.40 km/s indicated by Ackermann [1979] and 3.02 km/s indicated by Perkins et al. [1947] for these strata. Our smoothed velocity log from the INEL-1 well (Figure 2) indicates velocities of 4.9 km/s for the welded tuffs and 5.3 km/s for the recrystallized rhyodacite. The thicknesses of these layers were extrapolated from the well, this being the only lithologic reference point with velocity information near the intersection of the two seismic profiles.

#### Seismic Interpretation

Initially, the 136-km reversed seismic line from shotpoint 7 in the Northern Rocky Mountain (NRM) province to the Gay phosphate mine located in the Basin and Range (BR) province was interpreted. Shotpoint 7 was located 30 km northwest of the ESRP boundary. The Gay Mine is located 20 km southeast of the southern margin of the ESRP near Blackfoot, Idaho (Figure 1).

The data from both of these shotpoints were modeled iteratively. Figures 3 and 5 show the idealized crustal velocity models, to a distance of 70 km from the respective shotpoints, which provided appropriate fits to the arrivals on the seismic data. Also shown are representative computer-drawn ray paths used in generating the various calculated travel time curves utilized during the modeling. A complete model of the crustal structure across the ESRP was formed from the combination of the 70-km segments. Representative refracted and reflected phases from the top of the 6.53-km/s layer and the lower crustal 6.80-km/s layer are shown in the 136-km-long crustal model in Figures 4 and 6. The Conda Mine data were then used to extend this crustal model into the Basin and Range province southeast of the ESRP.

Because of the complexity of the inferred structure, the various groups of modeled rays are referred to as wave types or phases and denoted alphabetically. This provides a simple means of indexing the different phases with

their respective arrivals on the seismograms. Figures 4 and 6 display the theoretical travel time curves superimposed on the observed seismic sections recorded from shotpoint 7 and the Gay Mine, respectively.

#### Shotpoint 7

Phase A in Figures 3 and 4 has an apparent velocity of 5.56 km/s to a distance of 30 km and was modeled essentially as a direct wave. Theoretically, the travel time curve for this phase should pass through the origin on the seismic data, but instead it exhibits a delay in intercept time of approximately 0.3 s. This delay is accounted for by 450 m of 1.5-km/s low-velocity material below the shotpoint located in Antelope Valley. At a distance of 30 km from the shotpoint, the ESRP boundary is encountered and phase A from 30 to 45 km displays an apparent velocity of 4.84 km/s. This lower-velocity segment was modeled by introducing a fault into the velocity model at the ESRP boundary which accounts for the apparent velocity of phase A and the time delay evident for phase C, as discussed below.

The thickness of the 5.56 km/s sedimentary strata directly adjacent to the north side of the ESRP is not well known. However, a review of the stratigraphic work done by Ross [1962] and Skipp and Hall [1980] indicates that the thickness is quite substantial. We regard the 3-km thickness indicated by the velocity model (Figures 3 and 4) for these strata as a conservative value. In actuality, some of the Precambrian and lower Paleozoic quartzites, which Ross describes, conceivably could propagate seismic energy with a velocity of approximately 6 km/s. It would be difficult to distinguish between these strata and the upper crustal crystalline layer, thus resulting in a shallower interpreted depth to this interface.

A very prominent feature of the shotpoint 7 seismograms displayed in Figure 4 is the absence of a well-developed arrival with an apparent velocity of 6.15 km/s extending into the ESRP. However, phase C, the critical refraction from the top of the upper crust northwest of the SRP margin propagated through the normal fault at the ESRP boundary (Figure 3), matches the first arrivals on the seismograms between 30 and 55 km. We assumed the simplest structural model consistent with the data in generating this interpretation. The interface between the 4.90 and 5.30 km/s volcanics was projected from the well log location to the margin of the ESRP.

The seismic data available for the crossline do not provide definitive resolution on the depth to the bottom of the 5.30-km/s volcanics. The depth of approximately 5 km was derived by modeling of the crossline data while requiring reasonable consistency with the interpretation of the axial profile [Braille et al., this issue].

Phases D and E, reflections and refractions, respectively, from the top of the 6.53-km/s layer, indicate that this boundary slopes to the northwest with a dip of approximately  $10^\circ$ , as shown in Figures 3 and 4. The model indicates a depth of 7 km near the center of the plain and a depth of 17 km under shotpoint 7 to the top of this layer. However, phase D is only

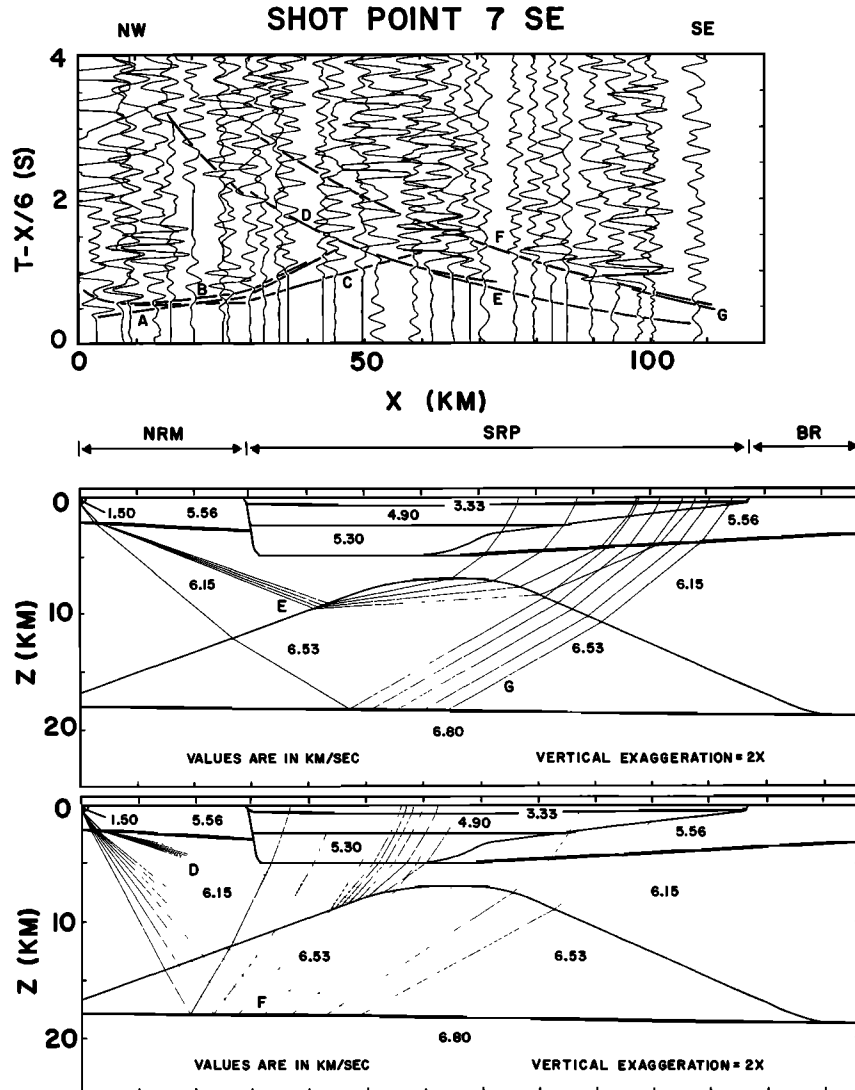


Fig. 4. Velocity model and calculated ray paths for larger distance range for shotpoint 7 to the southeast. Reduced-velocity seismic record section (top figure) shows the vertical-component seismograms, amplitude-normalized and plotted with an amplitude scaling factor of distance to the 1.5 power. Theoretical travel time curves for the phases illustrated in the velocity model (and from Figure 3) are also shown.

well developed from 27 to 70 km on the seismic record sections, and therefore, the configuration of this interface beneath shotpoint 7 is only inferred. These two phases produce the prominent arrivals between 60 and 70 km on the SP7 record section.

Finally, phase F, which is well developed from 70 to 110 km, was satisfactorily modeled as a reflection from the top of the 6.80-km/s layer. This interface dips slightly to the southeast from a depth of 18 km under shotpoint 7 to 19 km under the Gay Mine shotpoint. The calculated travel time curve for phase G, the theoretical head wave from this boundary, is also shown in Figure 4.

#### Gay Mine Shotpoint

The procedure used in the interpretation and the discussion of the Gay Mine data in this sec-

tion is analogous to the presentation of the shotpoint 7 data. Figure 5 shows the derived crustal model from the shot origin to a distance of 70 km, and Figure 6 displays the seismograms recorded from the mine blast and the calculated travel time curves superimposed above the velocity model of the ESRP. The model in Figure 6 is identical to that utilized in Figure 4. However, the corresponding phases have different expression in the seismic data recorded from the Gay Mine and thus qualitatively indicate structural differences between the northwest and southeast margins of the ESRP.

The station spacing and data recovery beyond 35 km for this shot were quite good. However, the inability to locate adequate seismograph sites in the area of the Snake River and Blackfoot, Idaho, caused the lack of coverage in the distance range of 20 to 35 km. Also, it was not possible to obtain data between the Gay Mine

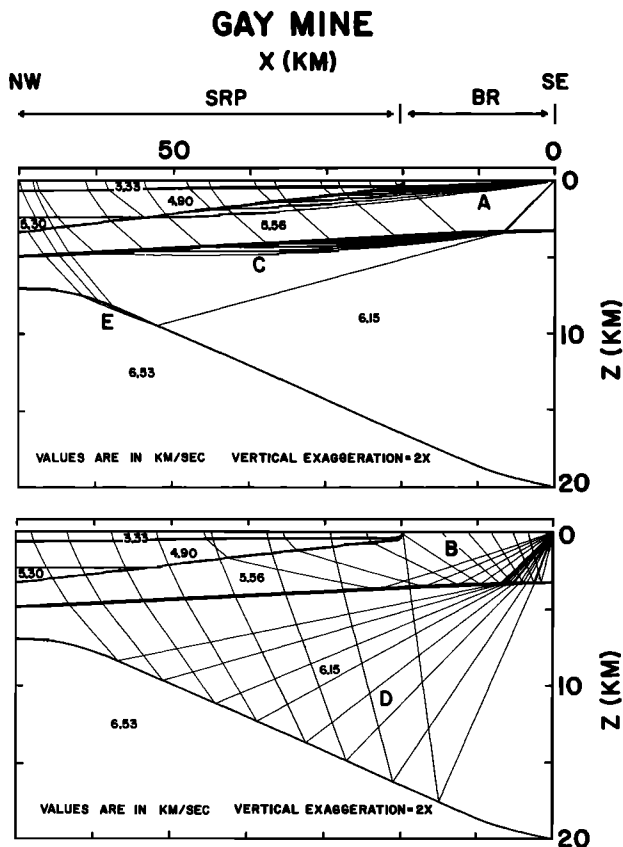


Fig. 5. Velocity model and ray paths for Gay Mine shotpoint to the northwest. Travel times for the refracted arrivals (upper figure) and reflected arrivals (lower figure) are shown in Figure 6.

shotpoint and the margin of the ESRP because of permitting difficulties. Thus, the velocity of the Paleozoic strata on the southeast side of the SRP is poorly defined. The velocity of 5.56 km/s was assumed for these rocks because it was consistent with the seismic data recorded from this shot and because it is the velocity associated with the corresponding rocks on the northwest side of the SRP.

Phase A in Figures 5 and 6 was modeled as a direct wave through the 5.56-km/s material to the ESRP boundary. At the margin, to allow for the fluvial deposits associated with the Snake River and the surficial basalts, a small fault of 500-m throw was modeled with the Paleozoic strata then dipping under the plain from this depth to a depth of 3.40 km at 70 km from the shot location. However, the location and throw of this fault is not well defined by the seismic data. Phase A then accounted for the 5.40-km/s apparent velocity arrival which is prominent on the seismograms extending across the plain from 35 to 53 km from the shotpoint (Figure 6).

The most striking difference between the shotpoint 7 and Gay Mine data is the presence of a first arrival with an apparent velocity of approximately 6 km/s on the Gay Mine record section. This arrival extends across the ESRP from approximately 35 to 80 km from the shot

location. An arrival analogous to this is totally absent in the shotpoint 7 data on the north side of the SRP and thus implies that the upper crustal layer extends under the southeast side of the ESRP relatively undisturbed.

The boundary between the 5.56-km/s material and the 6.15-km/s material was modeled as an interface dipping to the northwest from a depth of approximately 3 km under the Gay Mine in the Basin and Range province to a depth of 5 km near the center of the plain. Phases B and C in Figures 5 and 6 are the reflected and refracted arrivals from this interface.

Another very prominent arrival in the Gay Mine data is the large amplitude-reflected phase D, from the top of the 6.53-km/s layer. This phase provided substantial evidence for a sharp velocity contrast between the upper crustal layer and the 6.53-km/s material and the observations of this phase allowed accurate delineation of this interface. The travel times indicate that this interface is approximately 7 km deep near the center of the plain and dips to the southeast at 12° to approximately 19 km in depth beneath the Gay Mine.

The lower amplitude arrival approximately 0.5 s later than phase D was interpreted as the reflected arrival, phase F, from the top of the 6.80-km/s lower crust (Figure 6). Wave-type G, the refraction from this boundary, was calculated and the travel time curve shown, although the distance range of this profile precludes observation of this arrival. Also present in the seismic data for the Gay Mine shot is a large amplitude arrival approximately 1 s later than phase F between 53 and 90 km. Several unsuccessful attempts were made to adequately model this phase as a multiple arrival. It is possible that this phase is due to a phase which propagates as a shear wave for a portion of its ray path.

It should be added here that the available seismic data from shotpoint 7 and the Gay Mine do not allow definite resolution on the nature of the interface between the extension of the Paleozoic rocks under the ESRP and the 5.30-km/s volcanics in the region near the center of the plain. Modeling of record sections along the axis of the SRP [Braille et al., this issue] did not require the 5.56-km/s material to be present. Thus, the absence of the 5.56 km/s Paleozoic sedimentary rocks beneath the central and northeastern region of the SRP is reflected in our velocity model but cannot be inferred with certainty at this time. Figure 7 presents a record section from shotpoint 8 recorded transverse to the axis of the plain. A high-velocity (apparent velocity  $\approx$  6 km/s) first arrival is present on the record section beginning at about a distance of 30 km to the southeast. As can be seen by the rays calculated for the ESRP model (Figure 7), refractions from the top of the 5.56-km/s material under the plain provide a reasonable match to the observed arrivals. Owing to the small number of records available, the seismograms recorded to the northwest from shotpoint 8 were not interpreted. Also, the third through the seventh seismograms plotted on this record section to the southeast of the shotpoint were actually located parallel to the axis of the plain northeast of the shotpoint

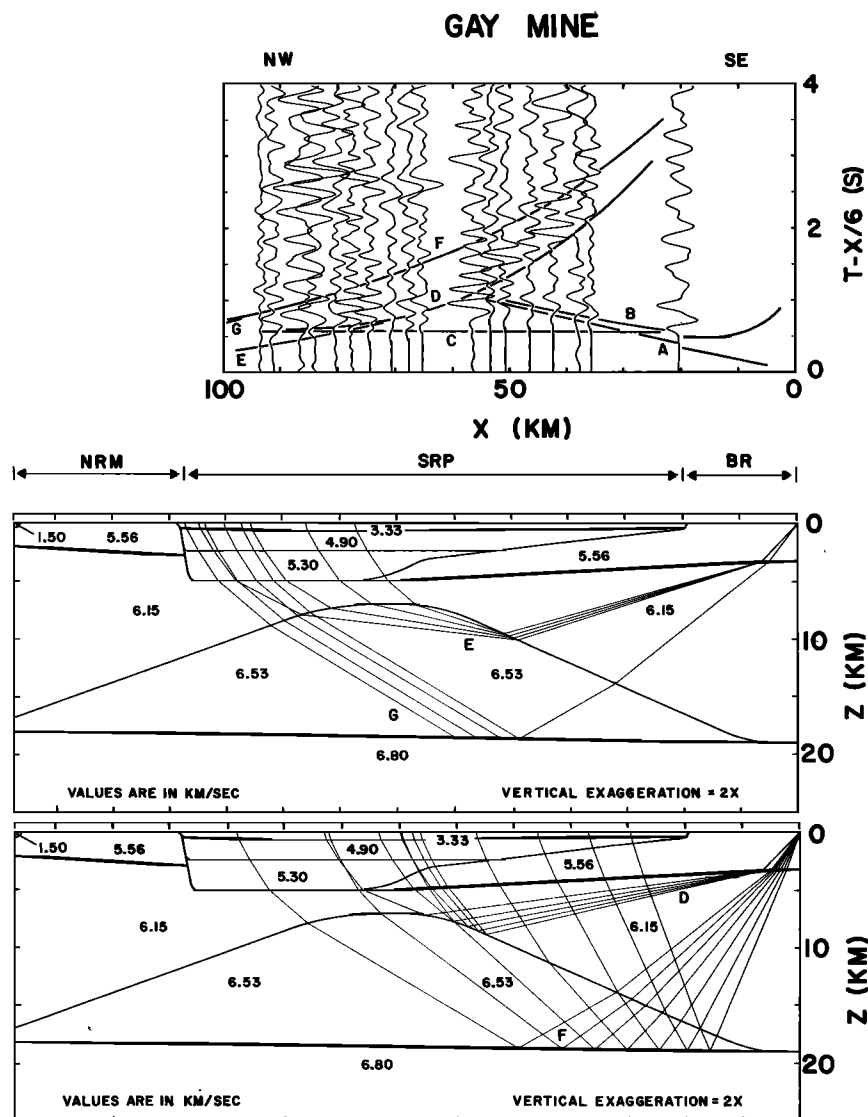


Fig. 6. Velocity model, ray paths, and seismic record section for larger distance range arrivals from the Gay Mine shotpoint. Record section shows vertical-component, amplitude-normalized seismograms with an amplitude factor of distance to the 1.5 power for plot scaling. Theoretical travel times are shown on the record section for the phases illustrated by the ray paths shown here and in Figure 5.

(Figure 1) and were modeled as shown in Figure 10, which is described later.

#### Conda Mine Shotpoint

The Conda Phosphate Mine is located approximately 59 km southeast of the Gay Phosphate Mine and 79 km southeast of the inferred SRP margin (Figure 1). As the Conda Mine shotpoint was not located in close proximity to the boundary of the ESRP, the data obtained from this blast were used primarily to determine the transition of deeper crustal layers between the Basin and Range province and the ESRP. Interpretation of the data for this line provided a model consistent with the shotpoint 7 to Gay Mine profile. However, the data were not useful in direct interpretation of the shallow structure of the ESRP.

The seismograms recorded from the Conda shot-

point and the derived model to a depth of 50 km are shown in Figures 8 and 9. The ray paths of the interpreted refracted phases are plotted on the idealized crustal model and the associated travel time curves are shown on the seismic record sections in Figure 8. The ray paths calculated for the various reflected phases are presented in Figure 9.

The crustal model shown in Figures 8 and 9, beyond a distance of 70 km from the Conda shotpoint, is exactly the model derived from the shotpoint 7 and Gay Mine interpretation. A low-velocity surface layer of 4.50 km/s dipping southeast near the Conda Mine was introduced to account for delay times of the arrivals. The calculated travel time curves for the direct wave through this layer and the reflected phase from the base of this material are shown on the seismograms in Figure 8, but they are not coded according to wave type. Thus, proceeding

## SHOT POINT 8 NW-SE

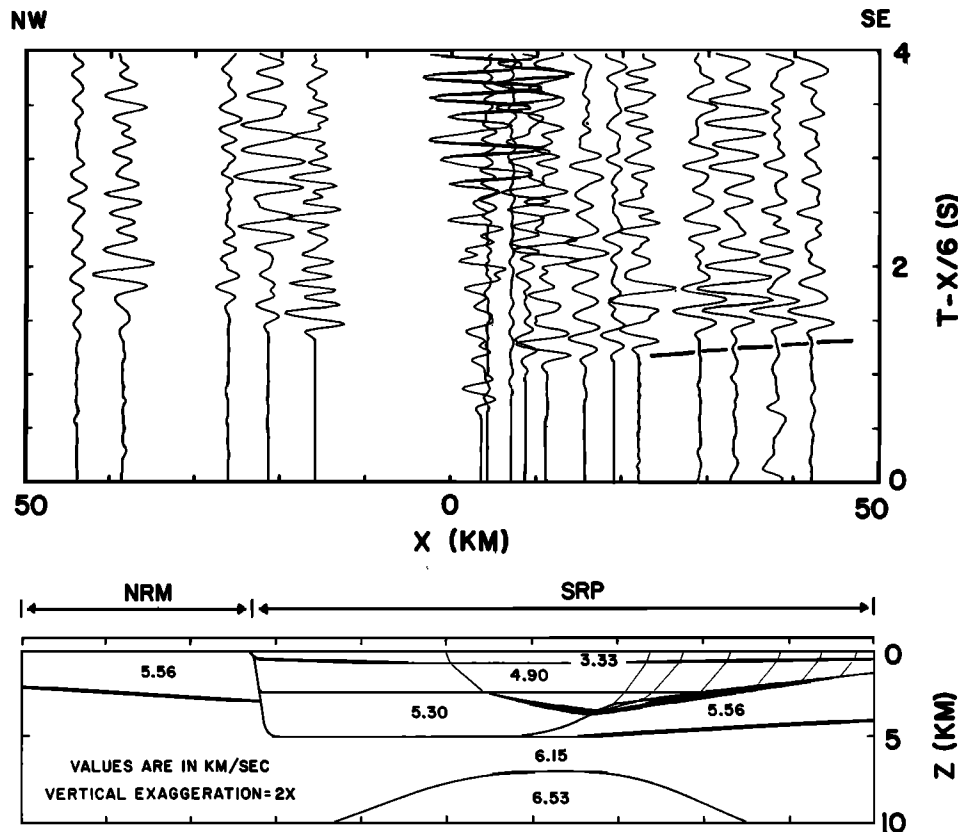


Fig. 7. Velocity model, ray paths, and seismic record section recorded from shotpoint 8 to the northwest and southeast. Theoretical travel times for the ray paths shown are drawn on the record section. The third through the seventh seismograms plotted to the right of the zero distance correspond to stations 2105, 2104, 2102, 2101, and 2652 (Figure 1), which are actually located northeast or east of the shotpoint and are modeled in Figure 10.

with phase A, the coding of the wave types is generally analogous to that previously discussed.

Phase A in Figure 8 is a refracted arrival from the 5.56-km/s layer representing the Paleozoic sedimentary rocks. Phase B is a reflected arrival from the top of the lower crust. Although some scatter in arrival times is evident in the distance range of 15-60 km due probably to station locations 'off-line' from the profile (Figure 1) and local near-surface velocity variations, these phases match the observed seismic data reasonably well.

From a distance of 40 km from the Conda shotpoint to the ESRP boundary the seismic data exhibit a first arrival with an apparent velocity somewhat higher than 6.15 km/s. By sloping the top of the upper crustal layer from 3.85 km in depth at a distance of 60 km to a depth of 6.35 km beneath the Conda Mine, phase C modeled these arrivals quite well with an apparent velocity of 6.25 km/s.

There is no evidence in the Conda Mine data that suggests the 6.53-km/s intermediate layer extends into the Basin and Range province for any appreciable distance. This interpretation of the crustal structure beneath the Basin and Range province, directly southeast of the ESRP margin, is consistent with the interpretation

of the American Falls Reservoir-Bear Lake-Flaming Gorge Reservoir seismic refraction data discussed by Wilden [1965]. His interpretation of the reversed profile, American Falls Reservoir-Flaming Gorge Reservoir, also did not require the presence of a layer with a velocity intermediate to the velocities of the upper and lower crust in this region.

Phase D, illustrated in ray paths and the travel time curve in Figure 8, is initially a reflection from the top of the lower crust and then becomes a reflection from the top of the 6.53-km/s layer. The triplication of the travel time curve caused by the structure of this interface is accompanied by large-amplitude arrivals on the observed record section.

Phases E and G are refractions from the top of the intermediate and lower crustal layers, respectively, and are shown in Figure 8. Phase G from the critical point to approximately 105 km has an apparent velocity of 6.80 km/s. Then from 105 km, the apparent velocity of this phase increases as the rays intersect the updip portion of the intermediate layer and then the apparent velocity decreases as the rays intersect the crest. Beyond 132 km, the apparent velocity is again approximately 6.80 km/s. The excellent correlation between the calculated arrivals of

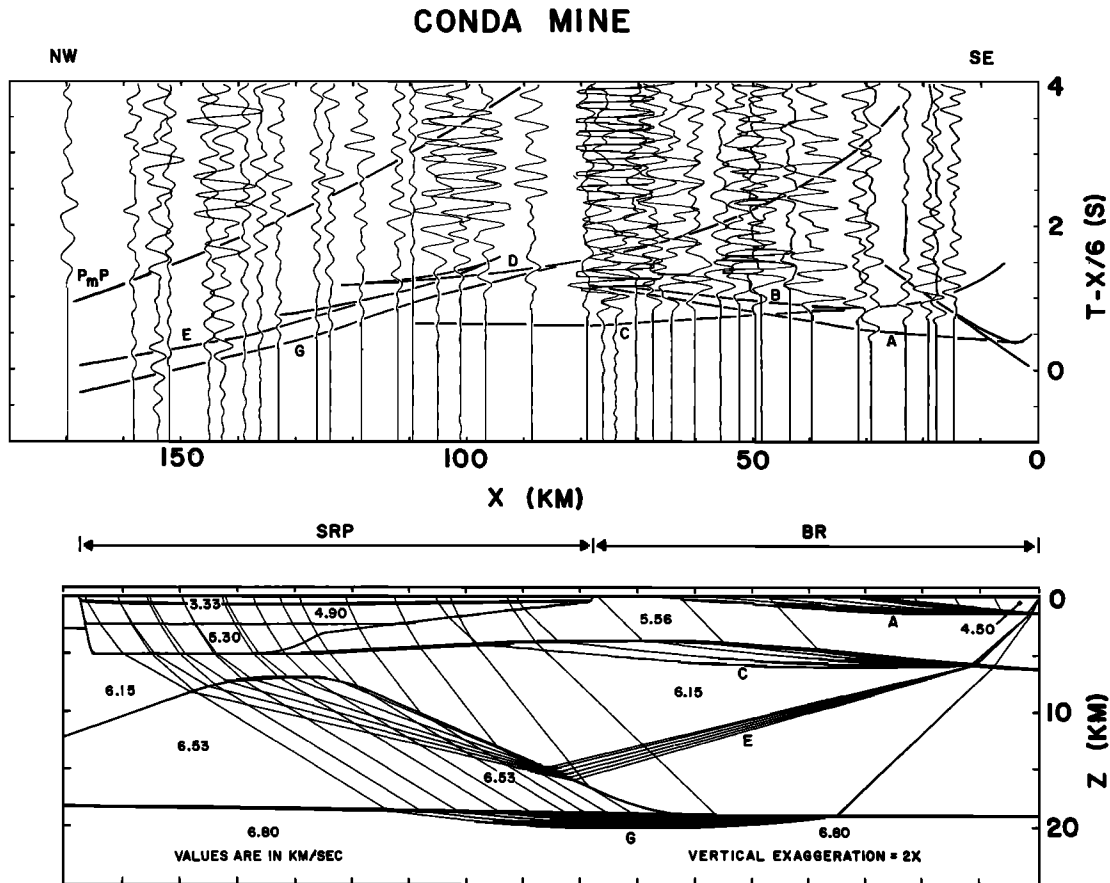


Fig. 8. Velocity model, ray paths for refracted phases, and seismic record section for the Conda Mine shotpoint. Record section shows vertical-component, amplitude-normalized seismograms with an amplitude scale factor of distance to the 1.5 power for plot scaling. Theoretical travel times are shown on the record section for the phases illustrated by the ray paths shown here and in Figure 9.

phase G and the actual seismic data from 110 to 160 km substantiates the configuration of the interface between the 6.53-km/s material and the lower crustal (6.80 km/s) layer beneath the ESRP. Thus, the Conda Mine data are in agreement with the shotpoint 7 and Gay Mine interpretation of this interface and are also consistent with the configuration of the 6.53-km/s layer as indicated by the shotpoint 7 to Gay Mine profile.

Finally, the reflected energy from the crust-mantle interface, indicated conventionally herein as PmP, is apparent in the seismic data beyond 110 km. This phase was modeled adequately with the Moho at 40 km in depth consistent with the interpretation of the PmP arrivals for the axial profile [Braille et al., this issue]. Although the model shown in Figure 9 indicates the interface is planar, reflections from this interface were obtained over only approximately a 30-km distance, and therefore the possibility of structure on this interface cannot be eliminated.

#### Shotpoint 8 NE and Shotpoint 4 SW

Shotpoint 8 NE and shotpoint 4 SW were recorded along the axis of the ESRP as a 47-km reversed refraction profile. Interpretation of this reversed profile provided the velocity

structure for the shallow crust near the center of the ESRP which was used to constrain the Conda-SP7 crustal model. Figures 10 and 11 show the seismic record sections from these two shotpoints to a distance of 50 km from their respective origins. The intersection of the shotpoint 7 to Gay Mine crossline with this profile is located approximately 15 km from shotpoint 8 (Figure 10) and approximately 32 km from shotpoint 4 (Figure 11).

Because a simple layered crustal model was used to model the shotpoint 8 NE and shotpoint 4 SW data, the phase nomenclature that is used in Figures 10 and 11 describes the reflected and refracted arrivals by the layer number from which the phase originates. Specifically, the refractions from the top of the  $i$ th layer are identified as  $P_i$ , while the reflections from the top of this layer are identified as  $P_iP$ . Because of the short distances involved, only the travel time curves associated with the first three layers are indicated on the seismic record sections, and only the  $P_3$  phase is represented by ray paths in the crustal model in both figures. The depths to the fourth and fifth layers were derived from the Conda-SP7 interpretation at the intersection with this profile. The interface between the 5.30-km/s material and the 6.15-km/s upper crustal layer may be highly

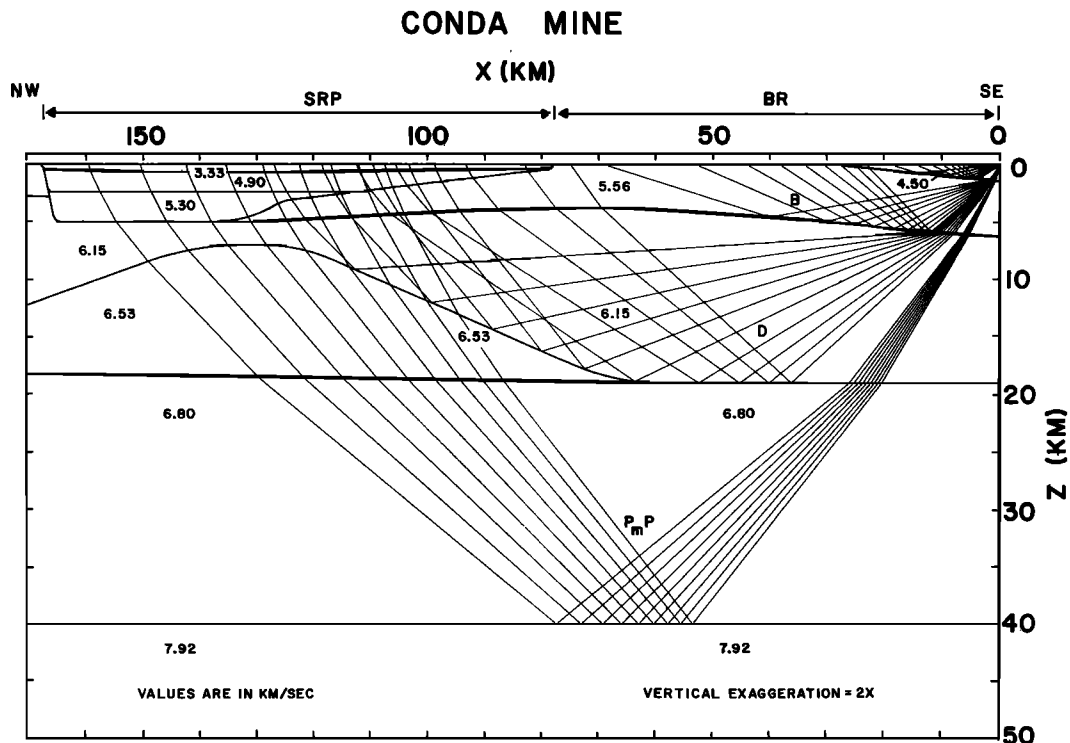


Fig. 9. Velocity model and ray paths for reflected phases for the Conda Mine shotpoint to the northwest. Travel times for these phases are plotted on the record section shown in Figure 8.

irregular if not gradational due to the nature of the volcanic processes which have probably produced this structure. There is also the possibility of the occurrence of  $\approx 5.56$ -km/s Paleozoic sedimentary rocks beneath the 5.3-km/s volcanic rocks, as discussed previously. However, presence of this layer was not required in the modeling of the axial line and could not be resolved with the 2- to 3-km station spacing used during data collection.

Computer modeling of this reversed profile yielded a velocity versus depth model of the crust which generally was in good agreement with the INEL-1 well interpretation (Figure 2). However, the modeling also indicated that significant relief existed in the interface between the 4.90- and 5.30-km/s material from approximately the midpoint of the profile to and beyond shotpoint 4. The surficial 3.33-km/s layer was modeled as 0.9 km in thickness beneath shotpoint 4. Layer 2, the 4.90-km/s material, was determined to be 2.7 km in thickness below shotpoint 8 and is essentially horizontal at this depth to a distance of 23 km from the shotpoint 8 location. For the next 24 km, this interface was modeled successfully as dipping  $4.5^\circ$  to a depth of 4.5 km beneath shotpoint 4. Preliminary modeling of shotpoint 4 NE, which is not presented here, suggests that the dip on this interface extends at least 30 km northeast of the shotpoint 4 location although with a somewhat lesser slope.

The  $P_2$  phase, refractions from the top of the 4.90-km/s welded-tuff layer, attenuate rapidly in amplitude, and energy from this arrival was essentially nonexistent in the seismic records beyond about 7 km from both of the shotpoint 8 and 4 locations. Thus, the

Q value of this material is extremely low [Braile et al., this issue].

The reflections and refractions from the top of the 5.30-km/s material, phases  $P_3P$  and  $P_3$ , respectively, account for the large amplitude early arrivals beyond about 10 km in both data sets. The  $P_3$  phase beyond approximately 27 km from shotpoint 4 (Figure 11) has an apparent velocity of approximately 5.30 km/s, as does the  $P_3$  phase between the critical point and 23 km from shotpoint 8 in Figure 10. Between the critical point for this phase to 27 km from shotpoint 4, the apparent velocity is greater than 5.30 km/s, while this phase exhibits an apparent velocity less than 5.30 km/s beyond 23 km from shotpoint 8. Thus the structure on the top of the 5.30-km/s material is inferred from these apparent velocity anomalies for the  $P_3$  phase.

#### Gravity Modeling

Several investigators have previously studied the gravity field associated with the ESRP and generally characterize the gravity field as an asymmetric positive anomaly roughly parallel to the axis of the ESRP [LaFehr and Pakiser, 1962; Mabey, 1976, 1978]. We calculated the gravitational field over the crustal model derived from the seismic interpretation and compared this field with observed gravity data to constrain further and refine the seismic modeling.

Three gravity profiles were constructed from a simple Bouguer gravity map provided by G. R. Keller (written communication, 1979) which was compiled from the gravity data file of the U.S. Defense Mapping Agency. The first profile

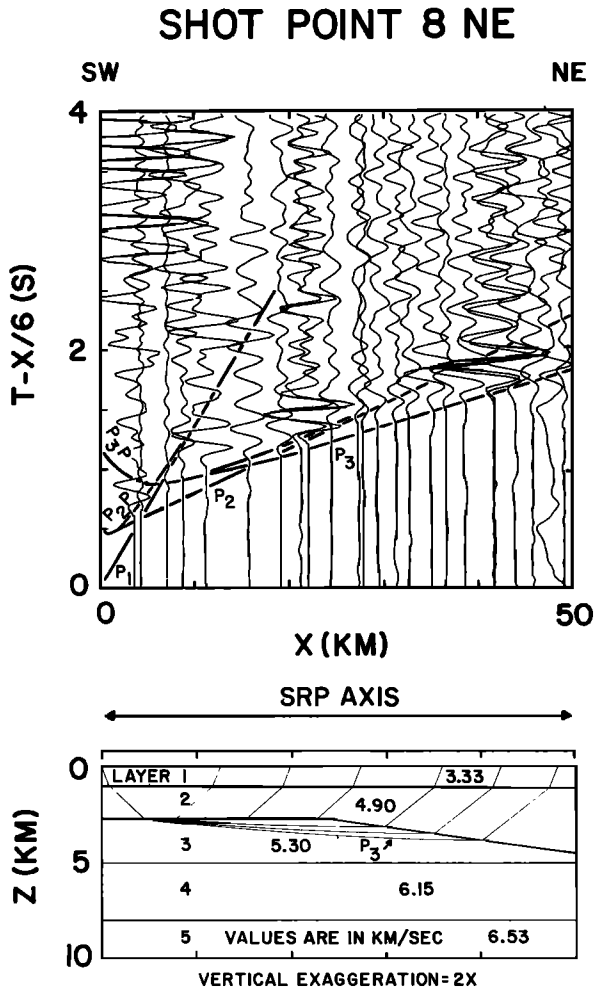


Fig. 10. Velocity model, ray paths (for the  $P_3$  arrival only), and seismic record section for shotpoint 8 to the northeast. Seismograms are vertical-component, amplitude-normalized with an amplitude scale factor of distance to the 1.5 power for plot scaling. Theoretical travel times for the velocity model are shown on the record section.

was coincident with the Conda-SP7 seismic profile and extended 50 km northwest of shotpoint 7 to 44°N latitude and 114°W longitude. This profile also extended 51 km southeast of the Conda Mine to 42°30'N latitude and 111°W longitude. The two other observed gravity profiles were of the same length (297 km) and parallel to the first one, however, they were located 20 km northeast and southwest, respectively, of the Conda-SP7 profile. By utilizing the three observed profiles, regional trends of the observed gravity field could be compared to the calculated gravity anomalies, and effects of localized density anomalies, which could not be resolved by either the seismic or the gravity data, could be minimized.

The densities assigned to the volcanic rocks were derived from an averaged, compensated density log recorded in the INEL-1 well. The remaining densities were determined by utilizing the appropriate seismic velocity versus density curves for various rock types compiled by Woollard

[1962]. The densities were assigned by selecting, from Woollard's velocity-density data, the average density value which corresponded to the seismic velocity for each layer. The velocity-density relation which resulted from this procedure is graphed in Figure 12. Although these densities were derived from various sources, this relation indicates that the velocity-density curve deviates very little from an almost linear relationship.

Figure 13 shows the topographic and gravity profiles above the final inferred geological model. The densities utilized in the calculation of the theoretical gravity curve are indicated in parentheses beside the corresponding seismic velocities. The general characteristics of the observed gravity profiles are matched quite well by the calculated profile, although no attempt was made to model the shorter-wavelength anomalies on these profiles. The fault structure on the northwest side of the SRP yields a characteristic-signature local anomaly which is

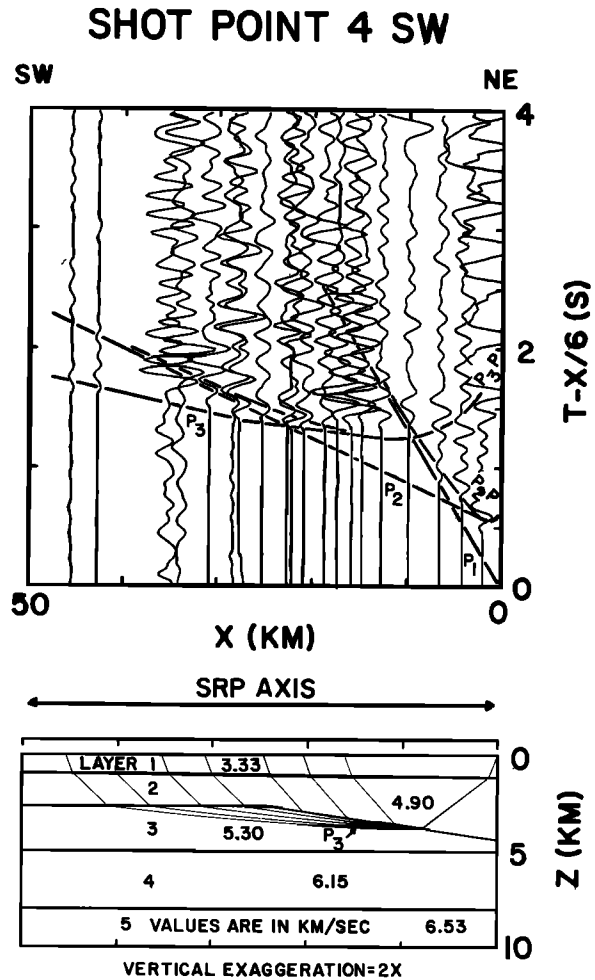


Fig. 11. Velocity model, ray paths (for the  $P_3$  arrival only), and seismic record section for shotpoint 4 to the southwest. Seismograms are vertical-component, amplitude-normalized with an amplitude scale factor of distance to the 1.5 power for plot scaling. Theoretical travel times for the velocity model are shown on the record section.

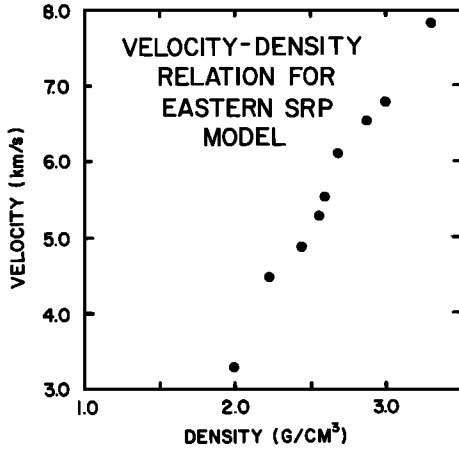


Fig. 12. Plot of velocity-density relation for the crustal model shown in Figure 13.

recognizable on the three observed gravity profiles although the amplitudes are slightly different and locations slightly shifted.

To model the gravity gradient northwest of the ESRP, it was necessary to thicken the lower

crustal layer in the idealized model from 10 km under the SRP to approximately 18 km northwest of the SRP margin. It also was necessary to decrease the distance that the 6.53-km/s intermediate layer extends beyond the northwest boundary of the plain to model satisfactorily the steep gravity gradient which occurs on this side of the plain. This configuration of the intermediate 6.53-km/s layer did not violate the seismic data, as there were no significant reflections observed from this region of the interface on the shotpoint 7 data. Also, the inferred crustal thickening to the northwest of the SRP is not constrained by the seismic data, and thus the gravity data could have equally well been modeled by a lower density crust rather than a variation in the depth to the Moho. However, the increased depth to the Moho in this area was the simplest structural assumption and is also consistent with isostatic compensation beneath the large topographic elevations associated with the Idaho Batholith and, therefore, was considered a reasonable assumption. The interfaces in Figure 13 are dashed where inferred and are solid where the seismic data were deemed sufficient to resolve them.

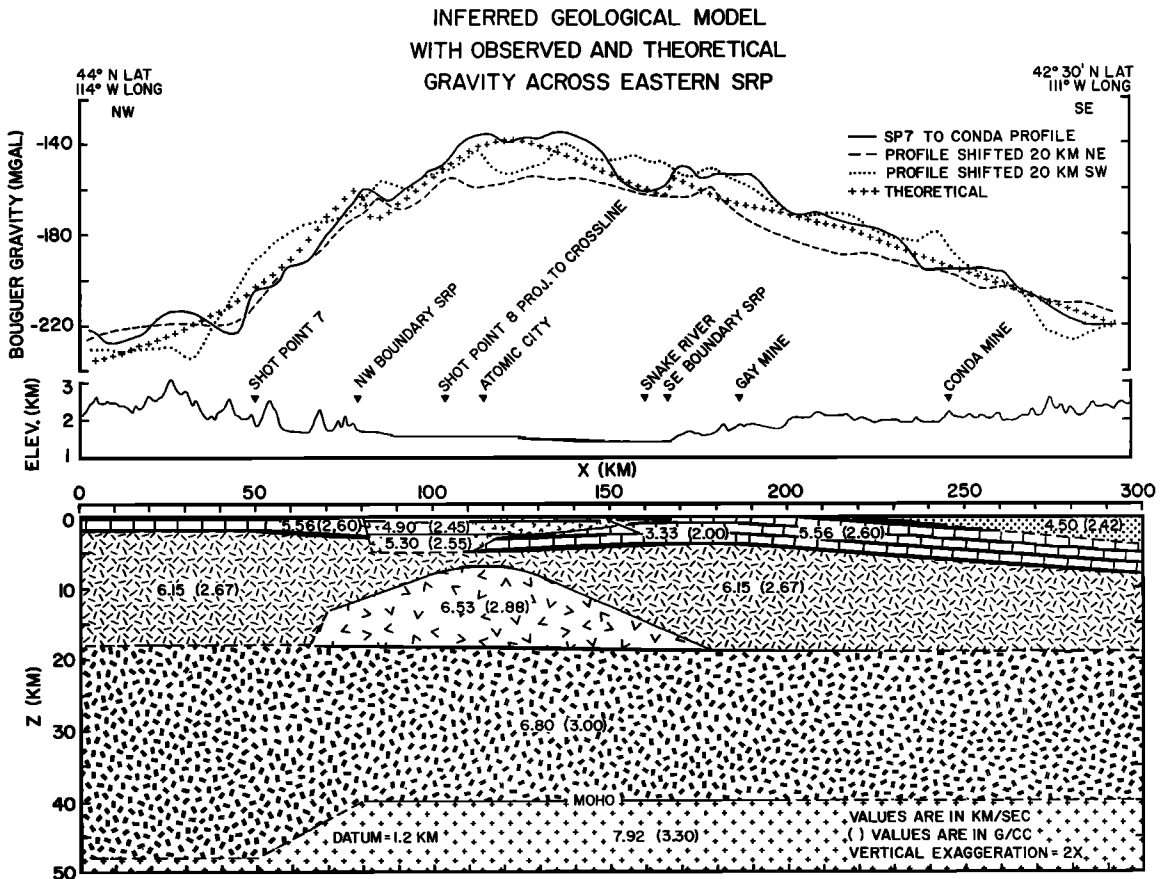


Fig. 13. Inferred crustal model across the eastern Snake River Plain. The datum for the crustal model is 1.2-km elevation. Interfaces are dashed where no seismic control is available. Elevation and gravity profiles are also shown. Three observed simple Bouguer gravity profiles are shown. One is located along the Conda-SP7 profile, and the other two are oriented parallel to the Conda-SP7 profile but are shifted 20 km northeast and 20 km southwest. The gravity anomaly calculated from the two-dimensional density model (densities are values shown in parentheses) is also illustrated.

### Conclusions

Use of the ray trace method to model the seismic refraction data presented here was invaluable in defining the crustal structure beneath the ESRP. The interpreted structural model presented in Figure 13 is consistent with the average crustal model parallel to the axis of the ESRP at their point of intersection [Braille et al., this issue]. However, simple dipping homogeneous layers were utilized in the modeling of the profiles along the axis of the ESRP, whereas the ray trace method utilized for the crossline provided information on the lateral variations of these layers and the structural transition associated with the margins of the ESRP.

The ray trace modeling of the seismic refraction profiles and subsequent gravity modeling has substantiated a three-dimensional idealized model of the crust beneath the ESRP and indicated the structure, especially in the upper crust, to be highly anomalous. An asymmetric grabenlike structure is indicated, with greater throw along the fault at the northwest margin of the ESRP. The graben is filled with a thick sequence of volcanic rocks. The 6.15-km/s upper crustal layer is greatly thinned in the ESRP in comparison with the surrounding regions.

The fault structure inferred at the northwest boundary of the ESRP, with the sedimentary strata terminating there, is a significant feature which was indicated by both the seismic and gravity data. However, it appears that along the southeast margin of the ESRP, the Paleozoic sedimentary rocks extend under the ESRP volcanics for a distance of at least 40 km. If there is a fault present along the southeast margin of the SRP, then it is of much less magnitude than that along the northwest boundary.

The modeling of the 6.53-km/s intermediate layer indicates that it is localized within the ESRP margins and has a minimum relief of 10 km above the contact with the lower crust beneath the center of the plain. This anomalous body may be interpreted as an intrusion of mafic material into the highly fractured upper crustal layer of the ESRP accompanying the graben formation or as a petrologic transition due to thermal metamorphism of the upper crust by a rising heat source. Whatever the process that has produced this anomalous body, it has resulted in an upper boundary of the body which is sharp enough to allow prominent reflections as observed on the Gay Mine record section. The lower boundary (top of the lower crustal layer) has also been preserved by this process, as indicated by the presence of reflected and refracted seismic phases from this interface and the fact that the interface can be traced into the adjacent geologic provinces in which the anomalous body is not found. Owing to the nature of this body and the recent volcanic history of the ESRP, we favor the intrusion process as illustrated schematically in Figure 14 as an explanation for the high-density and high-velocity crust in the ESRP.

The lower crust appears to be relatively undisturbed beneath the ESRP and is a continuous layer which extends into the adjacent geological provinces. The interpreted depth to the inter-

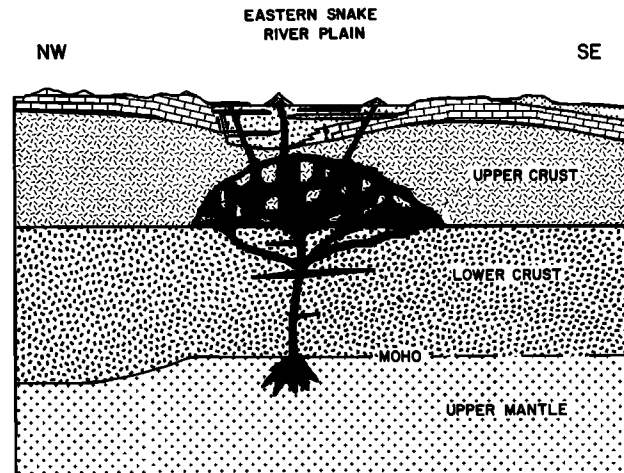


Fig. 14. Schematic diagram illustrating the inferred crustal model beneath the eastern Snake River Plain and adjacent provinces.

face between the upper and lower crust ( $19 \pm 1$  km) extending into the Basin and Range is consistent with the interpretation of the seismic refraction data between American Falls, Idaho, and Flaming Gorge, Utah, discussed by Willden [1965]. He found the depth to this interface from American Falls to Bear Lake to be 18.1 km, while the reversal of this segment of the profile indicated a depth of 19.4 km. Hill and Pakiser [1966] also interpreted the depth to the lower crust as 19 km beneath the Basin and Range province, south of the western SRP.

Combined gravity and ray trace travel time modeling has proven to be a powerful interpretation procedure for investigation of the crustal structure of the eastern Snake River Plain and the transition to adjacent provinces. A highly anomalous crust is shown to exist beneath the ESRP (Figure 14). A volcanic-filled asymmetric graben at least 5 km deep overlies an intruded upper crust beneath the ESRP. Proposed models for the geologic and tectonic evolution of the Snake River Plain should be capable of explaining this anomalous crustal structure.

**Acknowledgments.** We are grateful to all of the participants in the 1978 Y-SRP seismic refraction profiling experiment. Participants are indicated in the acknowledgments of the papers by Braille et al. [this issue] and Smith et al. [this issue]. The interest and hard work of these people in the field was critical to the success of the experiment and the interpretation presented here. We would especially like to thank the following people for helpful discussions during the course of this research: Mark R. Baker, Mike M. Schilly, Hans D. Ackermann, Jorg Ansorge, David D. Blackwell, Mel A. Kuntz, Roger Greensfelder, Kenneth H. Olsen, David P. Hill, John H. Healy, William J. Hinze, Claus Prodehl, John L. Sexton, S. Thomas Crough, and Walter Mooney. G. Randy Keller provided Bouguer gravity data for the eastern Snake River Plain. Walter Mooney provided us with a copy of the ray-tracing program used for the travel time modeling. The Idaho National Engineering Laboratory, the U.S. Forest Service, the National

Park Service, the U.S. Geological Survey, and the U.S. Bureau of Land Management were helpful with logistics in the field work. David Blackwell aided with the siting and acquisition of shot-point 8. Several government agencies and universities provided personnel and instrumentation during the experiment [see Braile et al., this issue; Smith et al., this issue]. Personnel at the Gay and Conda phosphate mines were most cooperative in allowing us to record the origin times of quarry blasts. The efforts of David Butler, Roger Bowman, Roger Grette, and Andy Staatz of Microgeophysics Corporation were important to the success of this experiment. This research was supported by the National Science Foundation grant EAR77-23357 to Purdue University and grant EAR77-23707 to the University of Utah and by the U.S. Geological Survey Geothermal Research Program grant 14-08-0001-G-532 to Purdue University.

## References

- Ackermann, H. D., Velocity structure to 3000-meter depth at the Idaho National Engineering Laboratory, eastern Snake River Plain (abstract), *Eos Trans. AGU*, **60**, 942, 1979.
- Baker, M. R., Application of time series analysis to the enhancement of seismic refraction data interpretation, M.S. thesis, Purdue Univ., West Lafayette, Ind., 1979.
- Baker, M. R., L. W. Braile, and R. B. Smith, Amplitude and phase normalization of seismograms from multiple seismograph recording systems for the Yellowstone-Snake River Plain seismic refraction experiment, *J. Geophys. Res.*, this issue.
- Braile, L. W., R. B. Smith, J. Ansorge, M. R. Baker, M. A. Sparlin, C. Prodehl, M. M. Schilly, J. H. Healy, St. Mueller, and K. H. Olsen, The Yellowstone-Snake River Plain seismic profiling experiment: Crustal structure of the eastern Snake River Plain, *J. Geophys. Res.*, this issue.
- Cerveny, V., I. A. Molotkov, and I. Psencik, *Ray Method in Seismology*, Vydala Universita Karlova, Praha, Czechoslovakia, 1977.
- Doherty, D. J., L. A. McBroome, and M. A. Kuntz, Preliminary geological interpretation and lithologic log of the exploratory geothermal test well (INEL-1), Idaho National Engineering Laboratory, eastern Snake River Plain, Idaho, *U.S. Geol. Surv. Open File Rep.*, 79-1248, 1979.
- Fenneman, N. M., and D. W. Johnson, Physical divisions of the United States, map, scale 1:7,000,000, U.S. Geol. Surv., Reston, Va., 1946.
- Hill, D. P., and L. C. Pakiser, Crustal structure between the Nevada Test Site and Boise, Idaho, from seismic-refraction measurements, in *The Earth Beneath the Continents, Geophys. Monogr. Ser.*, vol. 10, edited by J. S. Steinhart and T. J. Smith, pp. 391-419, AGU, Washington, D. C., 1966.
- LaFehr, T. R., and L. C. Pakiser, Gravity, volcanism and crustal deformation of the eastern Snake River Plain, *U.S. Geol. Surv. Prof. Pap.*, 450-D, 76-78, 1962.
- Mabey, D. R., Interpretation of a gravity profile across the western Snake River Plain, *Geology*, **4**, 53-56, 1976.
- Mabey, D. R., Regional gravity and magnetic anomalies in the eastern Snake River Plain, Idaho, *J. Res. U.S. Geol. Surv.*, **6**, 553-562, 1978.
- Perkins, B., D. S. Gardner, T. H. Pearce and R. M. Patterson, Subsurface structure of Snake River Valley, Idaho, from seismograph records of ammunition explosions (abstract), *Geophysics*, **12**, 496, 1947.
- Ross, C. P., Stratified rocks in south-central Idaho, *Pam. Idaho Bur. Mines Geol.*, **125**, 126 pp., 1962.
- Schilly, M. M., Interpretation of crustal seismic refraction and reflection profiles from Yellowstone and the eastern Snake River Plain, M.S. thesis, Univ. of Utah, Salt Lake City, 1979.
- Skipp, B., and W. E. Hall, Upper Paleozoic paleotectonics and paleogeography of Idaho, in *Paleozoic Paleogeography of West-Central United States*, edited by T. D. Fouch and E. R. Magathan, pp. 387-442, Rocky Mountain Section, Society of Economic Paleontologists and Mineralogists, Denver, Colorado, 1980.
- Smith, R. B., M. M. Schilly, L. W. Braile, J. Ansorge, M. R. Baker, C. Prodehl, J. H. Healy, St. Mueller, and R. W. Greensfelder, The 1978 Yellowstone-eastern Snake River Plain seismic profiling experiment: Crustal structure of the Yellowstone region and experiment design, *J. Geophys. Res.*, this issue.
- Willden, R., Seismic-refraction measurements of crustal structure between American Falls Reservoir, Idaho and Flaming Gorge Reservoir, Utah, *U. S. Geol. Surv. Prof. Pap.*, 525-C, 44-50, 1965.
- Woollard, G. P., The relation of gravity anomalies to surface elevation, crustal structure and geology, *Res. Rep. Ser. 62-9*, U.S. Air Force, Aeron. Chart and Inf. Cent., St. Louis, Mo., 1962.

(Received March 2, 1981;  
revised August 3, 1981;  
accepted August 21, 1981.)